



# Implantable composite devices of unsintered hydroxyapatite and poly-L-lactide with dispersive marbling morphology to enhance in vivo bioactivity and bioresorbability

Kazuaki Morizane<sup>a,\*</sup>, Yasuo Shikinami<sup>b</sup>, Shunsuke Fujibayashi<sup>a</sup>, Koji Goto<sup>a</sup>, Bungo Otsuki<sup>a</sup>, Toshiyuki Kawai<sup>a</sup>, Takayoshi Shimizu<sup>a</sup>, Shuichi Matsuda<sup>a</sup>

<sup>a</sup> Department of Orthopaedic Surgery, Graduate School of Medicine, Kyoto University, 54 Shogoin-Kawahara cho, Sakyo-ku, Kyoto, Japan

<sup>b</sup> Shikinami Yasuo Institute, 14 4F Lty932 1-1-1 Oji, Kusatsu, Shiga, Japan

## ARTICLE INFO

### Keywords:

Bioactive bioresorbable composite  
Hydroxyapatite  
Poly-L-lactide  
Marbling dispersion  
Forging reinforcement

## ABSTRACT

A bone fixation device made of unsintered hydroxyapatite (u-HA) particles uniformly dispersed in a poly-L-lactide matrix and reinforced by compressive forging (uniformly dispersed composite; UDC) has been clinically applied in several fields. However, it has reported some foreign body reactions over a long implantation period due to its slow bioresorbability. To further enhance its bioresorbability, we developed devices comprising a fibrous assembly of poly-L-lactide only three-dimensionally intertwined with particulate hydroxyapatite/poly-L-lactide composite. The biological behavior of the proposed material, provisionally referred to as complementarily reinforced composite (CRC), was compared with that of UDC in vivo. Cylindrical rods of UDC and CRC with 3.2-mm diameters were inserted bilaterally into the intramedullary distal femurs of 32 male Japanese white rabbits. Eight rabbits were euthanized at four, eight, 12, and 25 weeks after insertion. There were no significant differences between the mechanical properties of UDC and CRC over time. However, the results from histological analyses, surface characterization, radiological analyses, and push-out mechanical testing substantiated CRC's superior affinity to bone and enhanced bioactivity and bioresorbability in comparison with UDC. These characteristics were attributed to the dispersive marbling morphology produced by the CRC material's successive connectivity of u-HA particles throughout the PLLA matrix, which would accelerate PLLA hydrolysis degradation by H<sub>2</sub>O intrusion and enhance the bioactivity of u-HA particles exposed on the interface soon after implantation.

## 1. Introduction<sup>1</sup>

Various materials endowed with bioactivity and bioresorbability characteristics have been used clinically as bone fixation devices. One particularly successful example is a composite of unsintered hydroxyapatite (u-HA) and poly-L-lactide of which u-HA is uniformly dispersed in a poly-L-lactide matrix and reinforced by compressive forging (uniformly dispersed composite; UDC) to provide ultra-high strength over cortical bone [1,2]. This material is commercially available under the name OSTEOTRANS<sup>®</sup> or Super-Fixsorb<sup>®</sup>, and it has been widely used in orthopaedic [3–6], thoracic [7–9], maxillofacial [10–12], and

reconstructive [13] surgeries for > 20 years. This composite device has several advantages compared with similar implants fabricated by the other process, including maintaining its mechanical strength, [14,15] completely replacing surrounding bone tissue, [2] and easily detecting radiopaque devices as they are replaced by surrounding bone by means of X-ray images and/or computed tomography scans [1,2,16].

However, UDC have some disadvantages, including the long time required before the material is completely replaced with bone [2]. The bioresorption of composite devices proceeds through PLLA hydrolysis reactions. Because PLLA's methyl group side chain (–CH<sub>3</sub>) makes this component a hydrophobic polymer, the H<sub>2</sub>O molecules that cause

\* Corresponding author.

E-mail address: [morizane@kuhp.kyoto-u.ac.jp](mailto:morizane@kuhp.kyoto-u.ac.jp) (K. Morizane).

<sup>1</sup> Abbreviations:

BIC: bone implant contact

BV/TV: new bone volume to total volume

MAR: mineral apposition rate

u-HA: unsintered hydroxyapatite

<https://doi.org/10.1016/j.msec.2018.12.024>

Received 30 July 2018; Received in revised form 21 November 2018; Accepted 9 December 2018

Available online 10 December 2018

0928-4931/ © 2018 Elsevier B.V. All rights reserved.

hydrolysis cannot easily penetrate into the PLLA matrix, which imposes a rate limit on the reaction. H<sub>2</sub>O molecules naturally enter the material at the interface between the HA particles and the PLLA matrices. HA particles, with average diameters of 3–5 μm, are distributed in the PLLA matrix at 17/83 vol% (30/70 wt%) and are substantially separated from each other, which significantly reduces PLLA hydrolysis. The slow resorption can thus be attributed to the morphological structure of the HA particle dispersion, and the composite material therefore continues to produce an unpleasant sensation on the skin for a long time after implantation. With the thin plates and miniature screws used for the internal fixation of malar and midfacial fractures at shallow subcutaneous sites, mild side effects such as granulomas and surrounding edema have been found 3.5 years after intracranial neonatal skull fusion surgery, and fragments of large screw heads have been found in acetabular bone grafts 3–7 years after total hip arthroplasties [17,18]. Moreover, Landes et al. reported clinical outcomes after internal fixation of malar and midfacial fractures using HA-PLLA plates and screws, and 2 of 29 patients had a foreign body reaction that was treated by implant removal [19].

To minimize these complications, bioactive and bioresorbable devices with strength comparable to cortical bone should integrate with the surrounding bone soon after implantation, because the material's bioactivity promotes the direct bonding to bone that prevents positional displacement at the bone surface while retaining bone strength. Following implantation, PLLA degrades into fragments and is absorbed into the living body. The bone bonding occurs at the points contacting the osteoblasts where u-HA particles are exposed from the hydrolyzed PLLA matrix.

To address the limitations of current bone fixation devices, this article presents an implantable composite device with improved bioactive and bioresorbable behavior. We developed a novel composite, provisionally referred to as complementarily-reinforced composite (CRC), in which u-HA micro-particles connect successively throughout the PLLA matrix. In the proposed material, an assembly of PLLA-only fibers three-dimensionally intertwine with u-HA/PLLA composite fibers, such that u-HA particles are distributed from the surface to the back of the composite device. The purpose of this study was to investigate the mechanical, bioresorbable, and bioactive behavior of this novel composite, namely CRC, in comparison to UDC.

## 2. Materials and methods

### 2.1. Material preparation

The u-HA particles (HAP200) were supplied by Taihei Chemical Industrial Co., Ltd. (Osaka, Japan). The particle size was limited within a range of 0.3–20 μm, with an average size of approximately 3–5 μm. The Ca/P molar ratio was 1.67. PLLA was polymerized as previously described [1] and was supplied by Corbion Purac Co., Ltd. (Amsterdam, Netherland). The initial viscosity-average molecular weight ( $M_v$ ) of the PLLA powder was approximately 400 kDa.

We fabricated CRC rods according to the method described in United States patent number US-8900692-B2. The solution (A) consisted of PLLA pellets dissolved in dichloromethane at 2.0 wt%, and the solution (B) consisted of u-HA particles dispersed in (A). The concentration of solids was 3.0 wt%. The weight and volume ratios of u-HA/PLLA were 50/50 and 33/67, respectively. Each solution was sprayed from a gun nozzle toward a polypropylene net; (A) fibers were mixed crossly with (B) fibers in front of the net, so that the two types of fibers were intertwined three dimensionally into fabrics, which were then dried in air for 24 h. The fabrics were then melted at 190 °C, compressed under a reduced pressure, and cooled into a solid rod without voids. Finally, the rod was reinforced by compressive forging at 103 °C [1], and the composite rods were fabricated into final dimensions of 30 mm in length and 3.2 mm in diameter. The total weight ratio

of u-HA/PLLA in CRC was set at 30/70, equivalent to that of UDC. UDC rods were prepared for comparison following the previously reported method [1]. As for the surgical protocol in this study, we used the previous studies as references [20, 21].

### 2.2. Surface characterization

The surface morphologies and Ca/P distributions of UDC and CRC were examined by scanning electron microscopy (SEM) with energy dispersive X-ray spectroscopy (EDX) (S-4700; Hitachi Ltd., Tokyo, Japan) at an accelerating voltage of 10.0 kV after coating with carbon. EDX analyses were performed three times at different points and Ca/P ratio was calculated as the mean value.

### 2.3. Segmentation of u-HA/PLLA rods

To evaluate segments of the u-HA/PLLA composite, the composite rods were embedded in polyester resin. Sections (500 μm) were cut with a bandsaw (BS-300CP, EXAKT cutting system; Exakt Apparatebau GmbH, Norderstedt, Germany) perpendicular and parallel to the rod; these sections were ground to thicknesses of 60–80 μm using a micro-grinding MG-4000 (Exakt Apparatebau GmbH), and observed by microscopy (Eclipse 80i; Nikon, Tokyo, Japan) with a digital camera (DS-55 M-L1; Nikon, Tokyo, Japan). The specimens were also observed using SEM after coating with Pt/Pd.

### 2.4. In vivo experiments

#### 2.4.1. Animals

Thirty-two mature male Japanese white rabbits (weight: 2.5–3.0 kg) were used in this study, which was approved by the Animal Research Committee, Graduate School of Medicine, Kyoto University, Japan, following the guidelines of the National Institutes of Health Guide for Care and Use of Laboratory Animals (approval number: Med Kyo 18,258). All rabbits were radiologically analyzed; 16 of the 32 rabbits were mechanically tested, and the remaining 16 were histologically analyzed. Four time points were investigated (4, 8, 12, and 25 weeks); at each time point, four rabbits were subjected to mechanical testing of implants in two legs each ( $n = 4$ ), and four rabbits were subjected to histological analyses of implants in two legs each ( $n = 4$ ).

#### 2.4.2. Surgical procedure

Both UDC and CRC rods were sterilized with ethylene oxide gas at 50 °C for 5 h and were aerated for 7 days. The surgical methods used in this study were described previously [20,21]. In brief, the rabbits were anesthetized with an intravenous injection of pentobarbital sodium (40 mg/kg) (Kyoritsuuseiyaku Corp., Tokyo, Japan), an inhalation of isoflurane, and local administration of 0.5% (w/v) lidocaine solution (Pfizer Inc., NY, USA). The operations were performed under standard aseptic conditions [22]. A medial parapatellar incision was made, and the patella was laterally dislocated. A drill channel with a 3.2-mm diameter was then established through the intercondylar area of the distal femoral condyle using a dental bur with a 3.2-mm diameter (Morita, Kyoto, Japan). The opening of the drill hole was made in the intercondylar area 5 mm from the edge of the intercondylar notch. The cavity was washed thoroughly with a sterile saline, and the rods were inserted into the cavities with a press fit. UDC rods were implanted in one knee and CRC rods were implanted in the other knee of each rabbit. The capsule, the fascia, and the skin were sutured layer by layer.

#### 2.4.3. In vivo end points

The four rabbits in each group used for the histological analyses received calcein green (Sigma-Aldrich) subcutaneously both 14 and 7 days before necropsy to fluorescently label newly calcifying bone. At four, eight, 12, and 25 weeks after the operation, the eight rabbits in the respective groups were euthanized with an overdose of intravenous

pentobarbital sodium, after which segments of the bilateral distal femur containing the implants were cut and prepared for the radiological analyses, and mechanical or histological testing. All the specimens were kept moist after harvesting. To remove the bone growth at the rod insertion area, the bone tissue surrounding the entry point was carefully removed using a dental bur.

#### 2.4.4. Radiological analyses

All specimens were analyzed by a  $\mu$ -CT scan (SMX-100CT-SV-3; Shimadzu Corp., Kyoto, Japan), with a slice thickness of 0.04 mm. Three-dimensional images of harvested bone, including the implant rods, were reconstructed using a software package provided by the manufacturer (VG Studio MAX 2.2, Volume Graphics GmbH, Heidelberg, Germany). To evaluate the new bone volume surrounding the implants, a region of interest was established as a sphere with a 2.0-mm radius around a point 8 mm from the distal femoral insertion point. The same measurement conditions and error tolerances applied to all specimens. We calculated the ratio of the new bone volume to the defined total volume (BV/TV), where the new bone volume was defined as the region in the sphere with the same density as the cortical bone.

#### 2.4.5. Mechanical testing

**2.4.5.1. Push-out tests.** After performing the  $\mu$ -CT scans, push-out tests of the specimens were performed within 24 h of euthanasia to determine the bone-implant interface attachment strength. The push-out test was performed according to the modified method presented by Kettunen, et al. [23]. The push-out strengths of both UDC and CRC rods after implantation were measured using an Instron-type autograph (Model 1011; Aikoh Engineering Co., Ltd., Aichi, Japan) at room temperature (23 °C). A rigid configuration was used for the push-out tests (Fig. 1).

The sample orientation was adjusted carefully for every specimen so that the push-out direction was parallel to the contact surface between the implant and the bone [23]. The bone sample was gripped in the bilateral holder, and UDC and CRC rods were pushed out of the bone sample by a 2.0-mm-diameter blunt Kirschner wire gripped in a drill chuck (TR-4; Horiuchi MFG Co., Ltd., Ibaragi, Japan), using a crosshead speed of 20 mm/min. The maximum force, in Newtons, was used to characterize the adherence of the implant to the bone.

**2.4.5.2. Strength measurements.** After performing the push-out tests, we manually rinsed the surrounding tissue from the implant with 99.5% ethanol several times. The bending strength and modulus of both UDC and CRC rods were then measured by the three-point bending method, as previously described [21]. The procedure was performed according to the Japanese Industrial Standard using an Autograph AGS 200 D (Shimadzu Corp., Kyoto, Japan). The bending strength and modulus of the composite rods before implantation were also measured by similar methods ( $n = 4$ ).

#### 2.4.6. Surface analyses

After measuring the bending strength and modulus, we analyzed the surface of the samples using Fourier transform infrared spectroscopy (FTIR). FTIR analyses were performed at room temperature in the wavenumber range of 400–4000  $\text{cm}^{-1}$  (FT/IR-4200; JASCO Corp., Tokyo, Japan). The surfaces of the rods were sliced into approximately 200–300- $\mu\text{m}$  thicknesses with a sharp pointed scalpel, and subsequently pressed into discs.

#### 2.4.7. Molecular weight measurements

After analyzing surface topology, we measured each sample's molecular weight by determining the  $\bar{M}_v$  of PLLA after removing the u-HA particles by filtering with a solution of u-HA in dichloromethane at 25 °C.  $\bar{M}_v$  was determined using the Mark–Houwink formula [24]:



Fig. 1. Photograph of the push-out test. A femoral diaphyseal specimen with a composite rod as an intramedullary nail was gripped in the testing machine and pushed out by a Kirschner wire with a 2.0-mm diameter, at a crosshead speed of 20 mm/min.

$$[\eta] = 5.45 \times 10^{-4} \times M_v^{-0.73},$$

where  $[\eta]$  is the intrinsic viscosity measured at 25 °C using an Ostwald viscometer.

#### 2.4.8. Histological analyses

After the  $\mu$ -CT analyses, the specimens were fixed in 70% (v/v) ethanol for 14 days, dehydrated in serial concentrations of ethanol (80, 90, 99, and 100%) for 3 days at each concentration, and embedded in polyester resin. Sections (500  $\mu\text{m}$ ) were cut with a bandsaw perpendicular to the femoral axis and then micro-ground to thicknesses of 60–80  $\mu\text{m}$ . Several sections approximately 4–6 mm from the distal femoral insertion point were selected.

We first analyzed the surrounding new bone growth rate using fluorescence microscopy (BZ-X 710; Keyence Corp., Osaka, Japan) and BZ-X image analysis software to quantify the mineral apposition rate (MAR) at various bone depths along the implant margins [25,26]. Subsequently, each section was stained with Stevenel's blue and van Gieson's picrofuchsin (bright red) to stain soft tissue and calcified bone, respectively [27]. Thorough microscopic analyses were performed on the histological slides using a transmitted light microscope with a digital camera. The sections were evaluated by quantitative

histomorphometry to determine the amount of direct bone implant contact (BIC) ratio and degradation rate using Image J software (National Institutes of Health, USA). The BIC ratio was defined as the ratio of the length of direct contact between the bone and the implant to the total length of the implant. The degradation rate was defined as the difference between the device areas after and before implantation over time. To minimize the effects of fixation and dehydration, the device used to establish the pre-implantation value was fixed, dehydrated, and embedded in exactly the same way as that surgically implanted. The MAR, BIC ratio, and degradation rate were calculated after the tissue implant contact area had been manually defined. Each histomorphometric value was determined as the mean percentage of three consecutive sections. Finally, the biodegradability and bioactivity of the other thick sections of the implants were analyzed using SEM, after coating with Pt/Pd.

### 2.5. Statistical analysis

All data are shown as means  $\pm$  standard deviations. Statistically significant differences between the groups and time periods were subjected to one-way analysis of variance (ANOVA) followed by Tukey's honest significant difference tests. Significance was set at  $p < 0.05$ . All analyses were performed using JMP pro 13.0.0 (SAS Institute, USA).

## 3. Results

### 3.1. Surface characterization

Fig. 2(a) and (b) show the UDC and CRC screws, respectively, and Fig. 2(d) and (e) provide SEM images of the respective materials. In the UDC screw, the HA particles were distributed uniformly and the screw appears opaque in all segments, whereas in the CRC screw, HA particles were dispersed with a marbling distribution in the PLLA matrix of the fibrous layer, resulting in a mix of opaque and transparent areas. Fig. 2(c) shows the PLLA-only screw, which was entirely transparent, further supporting the CRC material's intermediate properties. In addition, EDX analysis showed that the Ca/P ratios of UDC and CRC were similar (1.75 and 1.78, respectively).

### 3.2. Distribution of *u*-HA

Fig. 3 shows the axial and sagittal sections of UDC and CRC. The CRC images show the specific structures formed by the connected distribution of the HA particles in the PLLA matrix, which resulted in the

marbling dispersions throughout the fibrous layer. In contrast, the HA particles in UDC were distributed uniformly and disconnectedly.

### 3.3. Radiological results

Fig. 4(a) shows the  $\mu$ -CT images that reveal the new bone formation surrounding the composite rods. At four weeks, thin new bone layers had formed around both UDC and CRC composite rods at the height of the epiphyseal plate. Moreover, the CRC's continuous marbling dispersions can be seen throughout all experimental periods. Fig. 4(b) shows the BV/TV ratio around the composite rods. CRC showed a higher ratio than UDC at every time; this was especially so after 25 weeks, whereas there were no statistical differences between the other groups.

### 3.4. Mechanical results

Fig. 5(a) shows the results of the push-out tests. In both UDC and CRC, the push-out strength gradually increased until 12 weeks after implantation. At 25 weeks, the push-out strength was relatively lower than at 12 weeks in both UDC and CRC. In UDC, the push-out strength at 12 weeks was significantly higher than at four weeks, and in CRC, the push-out strength at four weeks was significantly lower than at 12 weeks and at 25 weeks. UDC and CRC showed no significant differences at any given time point.

Fig. 5(b) shows changes in the bending strength of the composite rods over time. Both UDC and CRC retained 90% of their bending strength 25 weeks after implantation, and there were no significant differences between the groups and at any given time point.

### 3.5. FTIR analyses

Fig. 6 shows the FTIR spectra of the UDC and CRC surfaces after the push-out tests. Both UDC and CRC surfaces exhibited characteristic bands for  $\text{PO}_4^{3-}$  (1036, 1085, and  $1181\text{ cm}^{-1}$ ), and  $\text{CO}_3^{2-}$  ( $1381$  and  $1450\text{ cm}^{-1}$ ) containing HA. As for PLLA, there was a band at  $1758\text{ cm}^{-1}$  characteristic of the C=O stretching region in both SF and CRC, which contained both monocrystalline and crystalline phases of PLLA. The bands at  $2852$  and  $2923\text{ cm}^{-1}$  were also characteristic of  $-\text{CH}_2-$  or  $-\text{CH}_3$ , which are included in PLLA fibers. The spectra also show a short but wide peak at  $3000$ – $3700\text{ cm}^{-1}$  for both surfaces; however, this peak was more pronounced in CRC than in UDC especially at four and eight weeks. This result indicated increased OH<sup>-</sup> in the CRC material, resulting from the hydrolysis of surface PLLA.

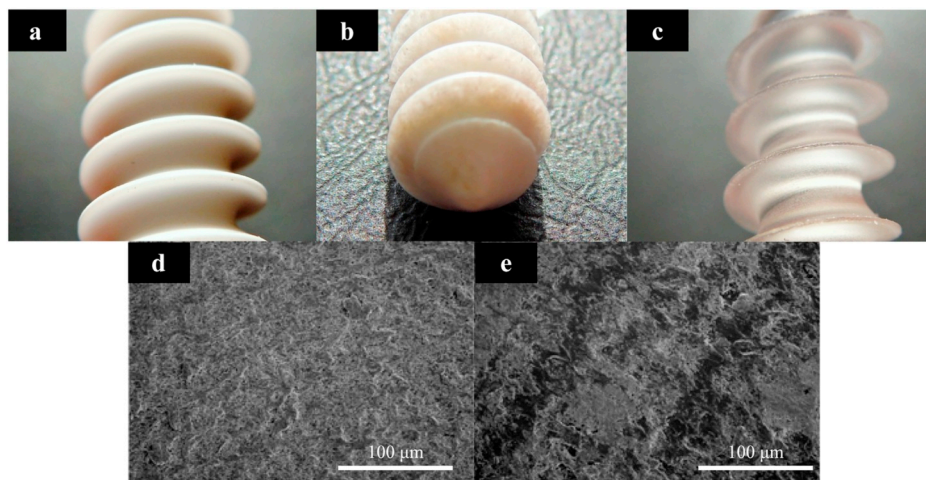


Fig. 2. The appearance of (a) UDC, (b) CRC, and (c) PLLA-only screws. The UDC screw appears opaque and the PLLA-only screw is transparent, while CRC appears to be a mix of opaque and transparent areas due to the distribution of HA particles. SEM images of the (d) UDC and (e) CRC surfaces.

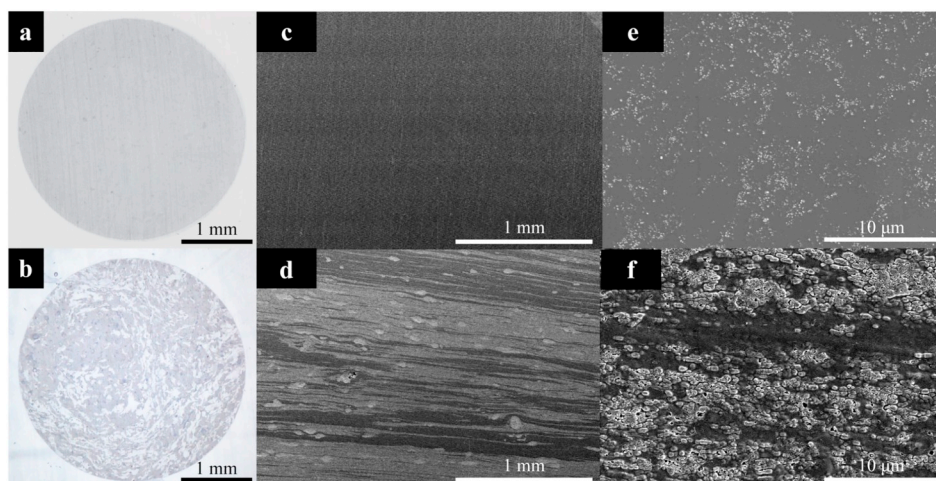


Fig. 3. Optical microscope images of (a) UDC and (b) CRC, and SEM images of (c, e) UDC and (d, f) CRC.

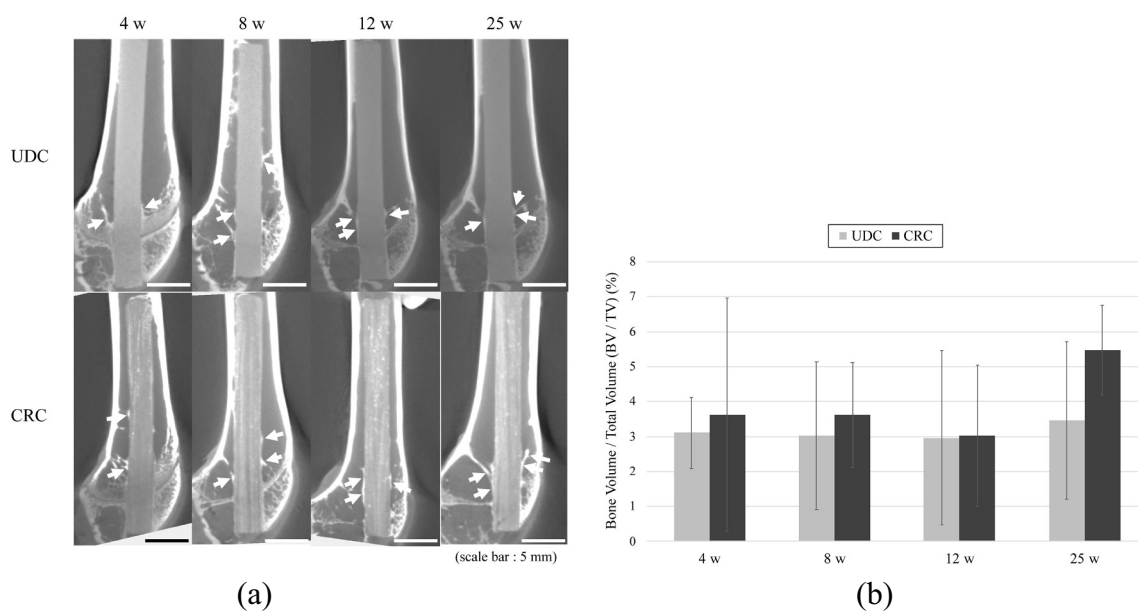


Fig. 4. (a) In vivo  $\mu$ -CT imaging of UDC and CRC at four, eight, 12, and 25 weeks. The arrows indicate the thin new bone layers formed around both materials at the height of epiphyseal plate. (b) Ratios of new bone volume to total volume (BV/TV) around the composite rods.

### 3.6. Molecular weight analyses

Fig. 7 shows changes in molecular weight of CRC over time. During the manufacturing process, the  $\bar{M}_v$  of PLLA was decreased from 400 kDa to approximately 250 kDa. Although the CRC's bending strength was approximately 93% of its initial value at 25 weeks, the molecular weight of the composite rod had dropped to approximately 20% of the initial value.

### 3.7. Histological results

We first analyzed the bone mineral apposition by measuring the dual labeling of the bone to determine the bone viability around the implant rod. Fig. 8(a) shows the MAR results, which reveal a higher MAR in CRC than in UDC at eight weeks. In addition, the MAR in CRC at eight weeks was significantly higher than that in CRC at 12 and 25 weeks.

Fig. 8(b) shows sections of histological specimen under high magnification after staining. No inflammatory responses appeared around

the rod throughout the experimental period. At four weeks, new bone formation was found around the composite rods of both UDC and CRC, with significantly more direct bone contacts in CRC than in UDC. At eight weeks, more new bone formation was found to partially deform the rod's periphery. At 12 weeks, mature bone was found to be directly bonded to the implant surface and penetrated into the CRC rod's periphery, but this was not observed with UDC. The CRC rod showed significantly more osteointegration than the UDC rod. At 25 weeks, more mature bone had penetrated to the CRC rod's periphery, and its overall shape was distorted, while that of UDC was almost as round as it had been initially, as shown in Fig. 8(c). Fig. 8(d) shows the BIC ratios, where significant differences can be seen between UDC and CRC at four and 12 weeks.

The degradation rate in CRC increased with time, as shown in Fig. 8(e). In contrast, the degradation rate in UDC was nearly unchanged and did not increase significantly. The degradation rates in CRC at eight, 12, and 25 weeks were significantly higher than those of UDC, whereas they were similar at four weeks. No apparent inflammation was found throughout the period.

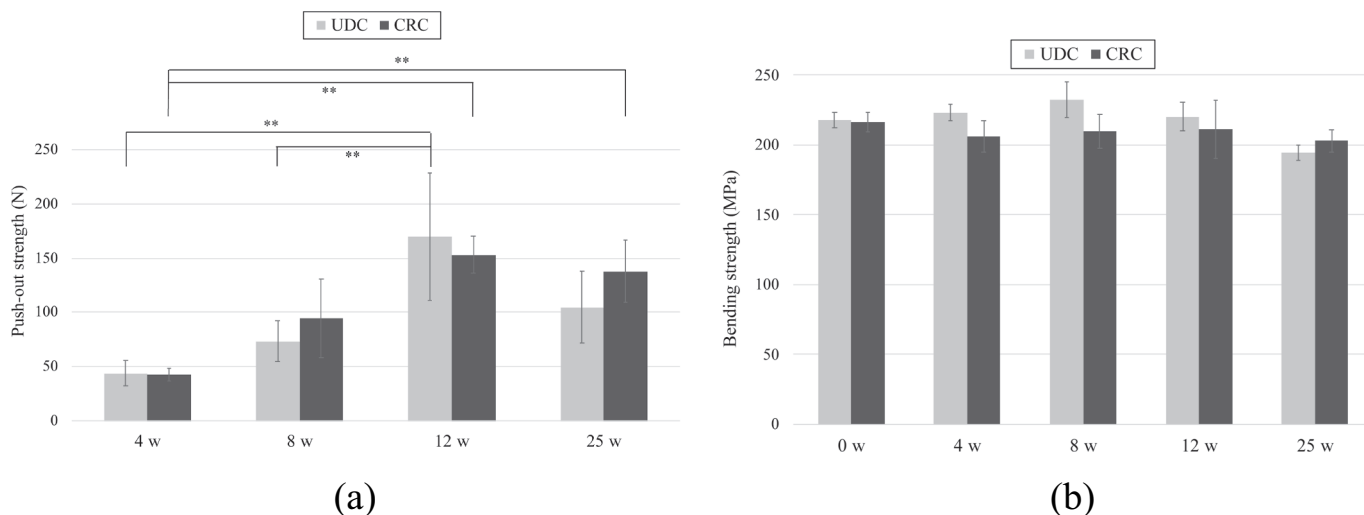


Fig. 5. Mechanical properties of UDC and CRC: (a) push-out test results and (b) bending strength results (\*:  $p < 0.05$ , \*\*:  $p < 0.01$ ).

Fig. 9 shows representative SEM images of the interface between the CRC rod and surrounding bone at eight and 12 weeks. At eight weeks, a thin layer of new bone had formed from the outside of the rod and along the PLLA layer. At 12 weeks, the length and width of the new bone formation in the rod was larger than at eight weeks.

#### 4. Discussion

This study investigated the mechanical, bioresorbable, and bioactive behavior of CRC compared with that of UDC in rabbits. We developed CRC composites comprising mixtures of PLLA-only fibers and particulate u-HA/PLLA to enhance bioactivity and bioresorbability. The dispersive marbling morphology exhibited by the CRC material was considered to result from the three-dimensional intertwining of the different fibers, whereby u-HA particles were distributed throughout the PLLA matrix at a ratio of 33/67 by volume (50/50 by weight), which established continuous particle connection throughout the matrix, as detected by SEM. CRC was complementarily endowed with rigidity and ductility by compressive forging reinforcement and the experiments indicated that hydrolysis reactions were promoted by H<sub>2</sub>O intruding through the interface between continuous u-HA particle layers and PLLA matrices to accelerate bioresorbability (Fig. 8(e)) and bioactivity (Fig. 8(a)-(d)), as shown in the FTIR spectra (Fig. 6). The overall ratio of u-HA in the CRC was equivalent to that in UDC (30/70 weight ratio), and CRC's mechanical properties, degradation rate, bioactive (osteoconductive), and bioresorbable behavior were

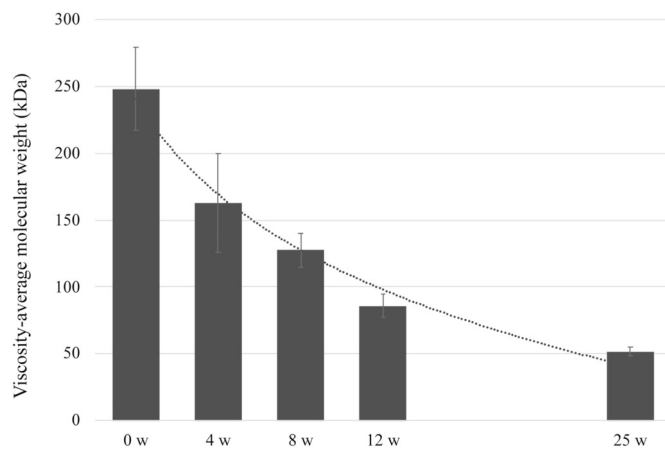


Fig. 7. CRC's molecular weight over time: the molecular weights at four, eight, 12, and 25 weeks were approximately 74, 56, 48, and 20% of the initial value, respectively.

improved as designed, which was substantially due to CRC's different morphology.

Bone fractures biologically require approximately three to four months to heal [28], and bone fixation devices should be integrated with bone just after implantation to prevent positional displacement at the bone surface and retain the natural bone strength until healing is

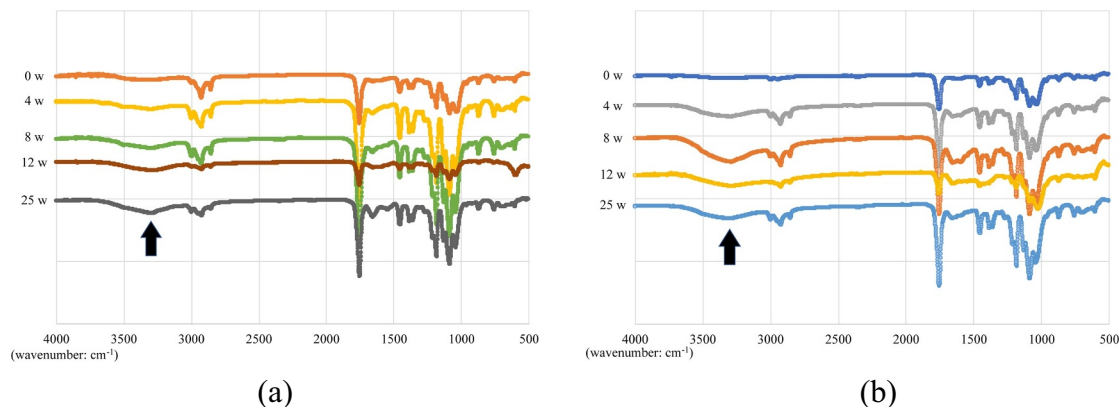
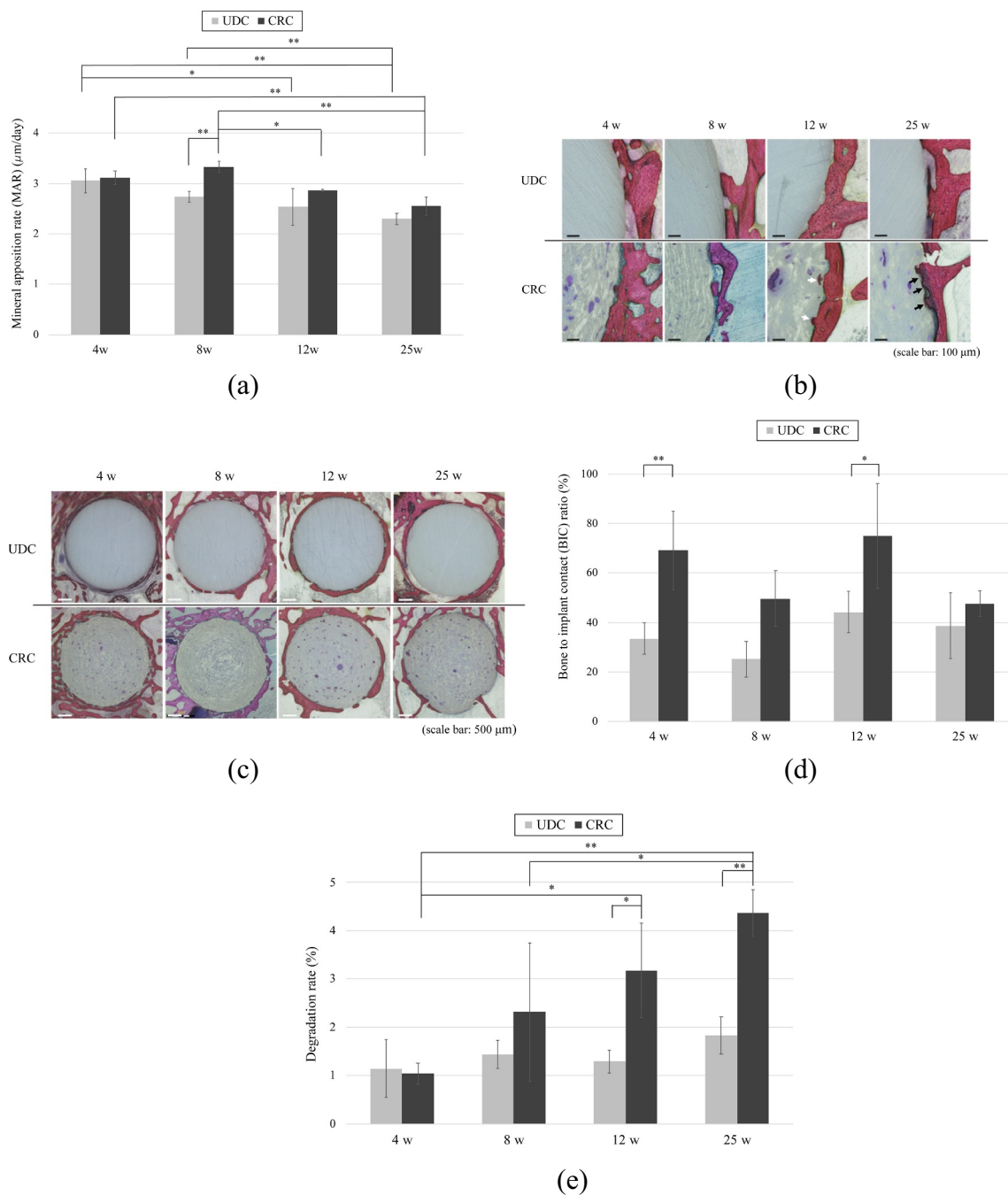


Fig. 6. FTIR spectra of (a) UDC and (b) CRC. The arrows indicate the short but wide peak at 3000–3700 cm<sup>-1</sup> that was more pronounced in CRC than in UDC.



**Fig. 8.** (a) MAR results for UDC and CRC. (b) High-magnification histological images of UDC and CRC. The white arrows in the CRC pane at 12 weeks show the unexpected formation of mature bone directly bonded to the implant surface and penetrated into the rod periphery, which was not observed with UDC. The black arrows in the CRC pane at 25 weeks indicate the increased penetration of mature bone into the rod's periphery, which distorted the rod's overall shape. (c) Low-magnification histological images. (d) BIC ratios (\*:  $p < 0.05$ , \*\*:  $p < 0.01$ ). (e) Degradation rates (\*:  $p < 0.05$ , \*\*:  $p < 0.01$ ).

complete. CRC showed sufficient bending strength and modulus at 25 weeks after implantation, with an average value of 203 MPa, comparable to that of cortical bone. Considering that the average initial strength of CRC was 217 MPa, CRC exhibited enough bending strength to act as bone fixation devices during the experimental period.

Although the results of the push-out tests and BV/TV did not show significant differences between the two types of implants, the BIC ratio was significantly higher in CRC at four and 12 weeks, and the MAR was also significantly higher in CRC at eight weeks than in UDC. UDC devices have been reported to contact directly with surrounding trabecular bone without any intervening fibrous tissue [29] only where the u-HA particles are exposed on the device surface, but not in the PLLA

matrix area. In contrast, this study showed a thin layer of new bone that migrated inside along the layer of fibrous PLLA and connecting u-HA particles layers at eight weeks in CRC. The results of the push-out tests and  $\mu$ -CT analyses at eight weeks indicated no significant differences between UDC and CRC, although CRC tended to show higher values than UDC. At 12 weeks, the layer of new bone migrating from the CRC surface to the inside became thicker (Fig. 8(b), 9), as observed by optical microscopy and SEM.

The CRC's molecular weight decreased over time, reaching 20% of the initial value after 25 weeks, which was similar to that of UDC as previously reported [21]. The FTIR analyses showed that CRC had a more pronounced peak than UDC at approximately  $3380\text{ cm}^{-1}$ ,

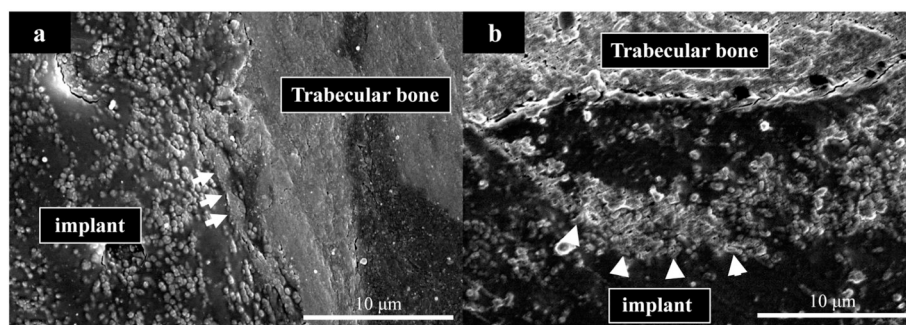


**Fig. 9.** SEM images of the interface between the CRC rod and the surrounding bone at (a) eight and (b) 12 weeks. The white arrows and arrowheads indicate new bone formation.

especially after four and eight weeks. These results indicate that in the degradation process of HA-PLLA devices, the amorphous layer of PLLA is preferentially degraded via hydrolysis [30] because of the easy intrusion of H<sub>2</sub>O molecules. As shown Fig. 8(e), the degradation rate in CRC at 25 weeks reached approximately 4%. Although UDC showed no complications during this study, CRC not only maintained bioresorbability but also exhibited no apparent complications including foreign body reactions. However, we could not evaluate the bioresorbability and bioactivity of CRC over a longer period in this study. Further study would be necessary for in CRC in longer period.

## 5. Conclusion

This study demonstrated that fibrous u-HA/PLLA layers in contact with surrounding bone in CRC were hydrolyzed preferentially, and that u-HA particles had increased opportunities to exhibit bioactivity. The small spaces generated along the fibrous u-HA/PLLA layers provided interconnected pores that accelerated intrusion and replacement with new bone in the latter stages of degradation. The characteristics of CRC described above could address the current limitations of UDC for long-term implantation. The components of u-HA/PLLA and the total weight ratio of 30/70 in both composite materials were equivalent, with only a morphological distinction in particle dispersion that improved the bioactivity and bioresorbability of CRC in comparison with UDC.

## Funding sources

No funds were received in support of this work.

## Conflict of interest

No benefits in any form have been or will be received from a commercial party related directly or indirectly to the subject of this manuscript.

## Acknowledgements

We greatly appreciate the technical support of Dr. Eenink Mart (Corbion Purac Co., Ltd) for the PLLA molecular weight analyses, Prof. Yoshiaki Hirano (Kansai University) for the FTIR analyses, and Mr. Haruyasu Kohda and Ms. Keiko Furuta (Kyoto University) for the electron microscopy study.

## References

- [1] Y. Shikinami, M. Okuno, Bioresorbable devices made of forged composites of hydroxyapatite (HA) particles and poly-L-lactide (PLLA): part I basic characteristics, *Biomaterials* 20 (1999) 859–877.
- [2] Y. Shikinami, Y. Matsusue, T. Nakamura, The complete process of bioresorption and bone replacement using devices made of forged composites of raw hydroxyapatite particles/poly L-lactide (F-u-HA/PLLA), *Biomaterials* 26 (2005) 5542–5551.
- [3] S. Uchida, H. Utsunomiya, T. Taketa, S. Sakoda, A. Hatakeyama, T. Nakamura, A. Sakai, Arthroscopic fragment fixation using hydroxyapatite/poly-L-lactide acid thread pins for treating elbow osteochondritis dissecans, *Am. J. Sports Med.* 43 (2015) 1057–1065.
- [4] Y. Arama, L.J. Salmon, K. Sri-Ram, J. Linklater, J.P. Roe, L.A. Pinczewski, Bioabsorbable versus titanium screws in anterior cruciate ligament reconstruction using hamstring autograft: a prospective, blinded, randomized controlled trial with 5-year follow-up, *Am. J. Sports Med.* 43 (2015) 1893–1901.
- [5] A. Sakai, T. Oshige, Y. Zenke, K. Menuki, T. Murai, T. Nakamura, Mechanical comparison of novel bioabsorbable plates with titanium plates and small-series clinical comparisons for metacarpal fractures, *J. Bone Joint Surg. Am.* 94 (2012) 1597–1604.
- [6] G. Kuroyanagi, H. Yoshihara, N. Yamamoto, H. Suzuki, K. Yamada, Y. Yoshida, T. Otsuka, N. Takada, Treatment of lateral tibial condylar fractures using bioactive, bioresorbable forged composites of raw particulate unsintered hydroxyapatite/poly-L-lactide screws, *Orthopedics* 41 (2018) e365–e368.
- [7] T. Ito, M. Kudo, R. Yozu, Usefulness of osteosynthesis device made of hydroxyapatite-poly-L-lactide composites in port-access cardiac surgery, *Ann. Thorac. Cardiovasc. Surg.* 86 (2008) 1905–1908.
- [8] Y. Tanaka, T. Miyamoto, S. Yoshitake, Y. Naito, Simple and useful method to minimize tracheal compression resulting from concave sternum during congenital heart surgery, *Ann. Thorac. Cardiovasc. Surg.* 100 (2015) 1901–1903.
- [9] T. Tsunekawa, A. Usui, H. Oshima, S. Mizutani, Y. Araki, N. Okada, Y. Ueda, A bioresorbable osteosynthesis device can induce an earlier sternal fusion after median sternotomy, *Interact. Cardiovasc. Thorac. Surg.* 15 (2012) 377–381.
- [10] S. Sukeyawa, T. Kanno, N. Katase, A. Shibata, Y. Takahashi, Y. Furuki, Clinical evaluation of an unsintered hydroxyapatite/poly-L-lactide osteoconductive composite device for the internal fixation of maxillofacial fractures, *J. Craniomaxillofac. Surg.* 27 (2016) 1391–1397.
- [11] C.A. Landes, A. Ballon, A. Tran, S. Ghanaati, R. Sader, Segmental stability in 24 orthognathic surgery: hydroxyapatite/poly-L-lactide osteoconductive composite versus titanium miniplate osteosyntheses, *J. Craniomaxillofac. Surg.* 42 (2014) 930–942.
- [12] K. Ueki, K. Okabe, K. Marukawa, A. Mukozawa, A. Moroi, M. Miyazaki, M. Sotobori, Y. Ishihara, K. Yoshizawa, K. Ooi, Skeletal stability after mandibular setback surgery: comparison between the hybrid technique for fixation and the conventional plate fixation using an absorbable plate and screws, *J. Craniomaxillofac. Surg.* 42 (2014) 351–355.
- [13] T. Kanno, H. Tatsumi, M. Karino, A. Yoshino, T. Koike, T. Ide, J. Sekine, Applicability of an unsintered hydroxyapatite particles/poly-L-lactide composite sheet with tack fixation for orbital fracture reconstruction, *J. Hard Tissue Biol.* 25 (2016) 329–334.
- [14] I. Balac, P.S. Uskokovic, R. Aleksic, D. Uskokovic, Predictive modeling of the mechanical properties of particulate hydroxyapatite reinforced polymer composites, *J. Biomed Mater Res B Appl Biomater* 63 (2002) 793–799.
- [15] H. Zhou, J.G. Lawrence, S.B. Bhaduri, Fabrication aspects of PLA-CaP/PLGA-CaP composites for orthopedic applications: a review, *Acta Biomater.* 8 (2012) 1999–2016.
- [16] Y. Shikinami, M. Okuno, Bioresorbable devices made of forged composites of hydroxyapatite (HA) particles and poly L-lactide (PLLA) part II: practical properties of miniscrews and miniplates, *Biomaterials* 22 (2001) 3197–3211.
- [17] Y.T. Katsuragi, A. Gomi, A. Sunaga, K. Miyazaki, H. Kamochi, F. Arai, N. Fukushima, Y. Sugawara, Intracerebral foreign body granuloma caused by a resorbable plate with passive intraosseous translocation after cranioplasty, *J. Neurosurg. Pediatr.* 12 (2013) 622–625.
- [18] K. Goto, Y. Okuzu, K. So, Y. Kuroda, S. Matsuda, Clinical and radiographic evaluation of cemented socket fixation concomitant to acetabular bone grafting fixed with absorbable hydroxyapatite-poly-L-lactide composite screws, *J. Orthop. Sci.* 21 (2016) 57–62.
- [19] C. Landes, A. Ballon, S. Ghanaati, A. Tran, R. Sader, Treatment of malar and mid-facial fractures with osteoconductive forged unsintered hydroxyapatite and poly-L-lactide composite internal fixation devices, *J. Oral Maxillofac. Surg.* 72 (2014) 1328–1338.
- [20] T. Furukawa, Y. Matsusue, T. Yasunaga, Y. Nakagawa, Y. Okada, Y. Shikinami, M. Okuno, T. Nakamura, Histomorphometric study on high-strength hydroxyapatite/poly(L-lactide) composite rods for internal fixation of bone fractures, *J. Biomed Mater Res B Appl Biomater* 50 (2000) 410–419.

- [21] T. Furukawa, Y. Matsusue, T. Yasunaga, Y. Shikinami, M. Okuno, T. Nakamura, Biodegradation behavior of ultra-high-strength hydroxyapatite/poly (L-lactide) composite rods for internal fixation of bone fractures, *Biomaterials* 21 (2000) 889–898.
- [22] T. Shimizu, S. Fujibayashi, S. Yamaguchi, K. Yamamoto, B. Otsuki, M. Takemoto, M. Tsukanaka, T. Kizuki, T. Matsushita, T. Kokubo, S. Matsuda, Bioactivity of sol-gel-derived TiO<sub>2</sub> coating on polyetheretherketone: in vitro and in vivo studies, *Acta Biomater.* 35 (2016) 305–317.
- [23] J. Kettunen, A. Makela, H. Miettinen, T. Nevalainen, T. Pohjonen, E. Suokas, P. Rokkanen, The fixation properties of carbon fiber-reinforced liquid crystalline polymer implant in bone: an experimental study in rabbits, *J Biomed Mater Res B Appl Biomater* 56 (2001) 137–143.
- [24] A. Schindler, D. Harper, Polylactide II. Viscosity–molecular weight relationships and unperturbed chain dimensions, *J. Polym. Sci. A Polym. Chem.* 17 (1979) 2593–2599.
- [25] K.D. Sinclair, T.X. Pham, D.L. Williams, R.W. Farnsworth, C.M. Loc-Carrillo, R.D. Bloebaum, Model development for determining the efficacy of a combination coating for the prevention of perioperative device related infections: a pilot study, *J Biomed Mater Res B Appl Biomater* 101 (2013) 1143–1153.
- [26] Z. Jones, A.E. Brooks, Z. Ferrell, D.W. Grainger, K.D. Sinclair, A resorbable antibiotic eluting bone void filler for periprosthetic joint infection prevention, *J Biomed Mater Res B Appl Biomater* 104 (2016) 1632–1642.
- [27] Y. Okuzu, S. Fujibayashi, S. Yamaguchi, K. Yamamoto, T. Shimizu, T. Sono, K. Goto, B. Otsuki, T. Matsushita, T. Kokubo, S. Matsuda, Strontium and magnesium ions released from bioactive titanium metal promote early bone bonding in a rabbit implant model, *Acta Biomater.* 63 (2017) 383–392.
- [28] K. Ito, S.M. Perren, Biology of fracture healing, in: T.P. Ruedi, R.E. Buckley, C.G. Moran (Eds.), *AO Principles of Fracture Management*, AO Foundation Publishing, Davos, 2013.
- [29] T. Yasunaga, Y. Matsusue, T. Furukawa, Y. Shikinami, M. Okuno, T. Nakamura, Bonding behavior of ultrahigh strength unsintered hydroxyapatite particles/poly(L-lactide) composites to surface of tibial cortex in rabbits, *J Biomed Mater Res B Appl Biomater* 47 (1999) 412–419.
- [30] H. Tsuji, A. Mizuno, Y. Ikada, Properties and morphology of poly(L-lactide) III. Effects of initial crystallinity on long-term in vitro hydrolysis of high molecular weight poly(L-lactide) film in phosphate-buffered solution, *J. Appl. Polym. Sci.* 77 (2000) 1452–1464.



**Koji Goto** was born in Osaka, Japan, in 1970. He received his M.D. in medicine from Kyoto University in 1995, and a Ph.D. degree from the Graduate School of Medicine, Kyoto University in 2006. In 1995, he started his career as an orthopaedic surgeon at Kyoto University Hospital. After he worked at several hospitals from 1996 to 2002 and from 2006 to 2011, he started to work at Kyoto University Hospital as the chief orthopaedic surgeon for hip surgeries as well as a lecturer. He researched on bioactive and bioresorbable materials and developed a new bioactive bone cement containing titania particles. For this outstanding research, he got the Japan Sigmaw Award in 2011.



**Bungo Otsuki** was born in Kyoto, Japan, in 1972. He received his M.D. in medicine from the University of Kyoto, Japan, in 1997, and Ph.D. degrees in medicine from the Graduate School of Medicine, Kyoto University, in 2007. In 2008, he joined the Kobe city General Hospital as the head physician for spine surgery. Since 2008, he has been with the department of orthopaedics, Graduate School of Medicine, Kyoto University, as an assistant professor. His current research interests include clinical spine surgery and the development of biomaterials suitable for spine surgery.



**Toshiyuki Kawai** is a material scientist and orthopaedic surgeon currently working for Kyoto University Hospital. He got his M.D. in 2003 and then was given his Ph.D. in 2013 at Kyoto University for his works on various chemical and heat treatments for Titanium metal. He also worked for Department of Orthopaedic Surgery at Stanford University until 2016. He was awarded to Young Investigator Award 2015 and served as a member of editorial board for the journal “Tissue Engineering”.



**Takayoshi Shimizu** was born in Osaka, Japan, in 1981. He received his M.D. from Kagawa University School of Medicine, Japan, in 2007, and his Ph.D. in orthopaedic bioengineering from Graduate School of Medicine, Kyoto University, in 2017. He is currently a staff spine surgeon at Kyoto University Hospital, Japan. His research interests include clinical outcome of minimally invasive spinal surgery, scoliosis, and bioengineering for the spinal implants.



**Shuichi Matsuda** is a professor and chairman at Department of Orthopaedic Surgery, Kyoto University. He graduated from the medical school of Kyushu University (Japan) in 1990, and took a research fellowship at Barnes West Hospital, Washington University in St Louis (USA). He completed his Ph.D. thesis on knee kinematics in 2002. In 2012, he was appointed as the chairman of the Department of Orthopaedic Surgery, Kyoto University. He has published > 300 peer reviewed articles and he is a member of many international societies such as Association of Bone and Joint Surgeons (ABJS), AAOS, ORS, among others.



**Kazuaki Morizane** was born in Osaka, Japan, in 1984. He received his M.D. from Kyoto University, Japan, in 2010. He is currently a graduate student and an orthopaedic surgeon in the Department of Orthopaedic Surgery at Kyoto University in Japan. His main areas of research interest are biomaterial engineering and spine surgery. He is a member of the Japanese Society for Biomaterials and Japanese Orthopaedic Association and received the best biology young investigator poster presentation award from the European Orthopaedic Research Society in 2017.



**Yasuo Shikinami** is a biomaterial scientist, NASS member and now a representative of Shikinami Yasuo Institute LLC. He received his Ph.D. from the Kyoto University in 1991 and academic awards of the Society of Polymer Science, Japan (1998) for his paper “Adhesive gel materials for medical uses” and of the Japanese Society for Biomaterials (2008) for his paper “Development of high strength of F-u-HA/PLLA composite devices and its clinical application”.



**Shunsuke Fujibayashi** is a professor at the Department of Orthopaedic Surgery in Kyoto University from 2015. He is a chief of both the spine surgery and the biomaterial research groups. He received his Ph.D. in 2003 from Kyoto University. In 2009, he studied abroad as the Japanese Welfare and Labor Ministry Visiting Fellow at Nantes University in France. His research interests in the area of biomaterials are bioactive ceramics and absorbable polymers. He has performed > 4000 cases of spine surgery and conducted many clinical researches. He has over 150 publications in various English journals.